Inorg. Chem. **2009**, *48*, 111−120

Structural Consequences of Anionic Host−Cationic Guest Interactions in a Supramolecular Assembly

Michael D. Pluth, Darren W. Johnson, Géza Szigethy, Anna V. Davis, Simon J. Teat, Allen G. Oliver, Robert G. Bergman, and Kenneth N. Raymond*

Department of Chemistry, University of California, Berkeley, California 94720-1460, and Chemistry Division, Lawrence Berkeley National Laboratory, Berkeley, California 94720

Received July 9, 2008

The molecular structure of the spontaneously assembled supramolecular cluster $[M_4L_6]^{n-}$ has been explored with different metals (M = Ga^{III}, Fe^{III}, Ti^{IV}) and different encapsulated guests (NEt_4^+, $BnNMe_3^+$, Cp_2Co^+, $Cp^*_2Co^+$) by X-ray crystallography. While the identity of the metal ions at the vertices of the M_4L_6 structure is found to have little effect on the assembly structure, encapsulated guests significantly distort the size and shape of the interior cavity of the assembly. Cations on the exterior of the assembly are found to interact with the assembly through either $\pi-\pi$, cation$-\pi$, or CH$-\pi$ interactions. In some cases, the exterior guests interact with only one assembly, but cations with the ability to form multiple $\pi-\pi$ interactions are able to interact with adjacent assemblies in the crystal lattice. The solvent accessible cavity of the assembly is modeled using the rolling probe method and found to range from 253−434 Å^3, depending on the encapsulated guest. On the basis of the volume of the guest and the volume of the cavity, the packing coefficient for each host−guest complex is found to range from 0.47−0.67.

1. Introduction

Much of the guest-binding specificity in supramolecular assemblies is derived from noncovalent interactions between the host and guest molecules, which can include Coulombic, van der Waals, hydrogen-bonding, or ion-association forces, as well as steric interactions, $\pi-\pi$, cation$-\pi$, anion$-\pi$, or CH$-\pi$ interactions. Such forces can be attractive or repulsive in nature and can act either independently or cooperatively. Although most of these forces are weak, their combination upon guest inclusion in synthetic host molecules can lead to strong and specific guest binding, chiral recognition,[1−5] stabilization of reactive intermediates,[6−9] and chemical catalysis.[10−13] These forces are not restricted to synthetic systems; they have been shown to have biological importance in enzyme active sites and the self-assembly processes of biological molecules.[14−18] Greater understanding of host−guest interactions may inform the design of systems with enhanced guest binding selectivities and better control over encapsulated reactivity.

The effects of host−guest intermolecular forces are often difficult to determine or deconvolute in solution because the

* To whom correspondence should be addressed. Fax: 510-486-5283. E-mail: raymond@socrates.berkeley.edu.

(1) Hembury, G. A.; Borovkov, V. V.; Inoue, Y. *Chem. Rev.* **2008**, *108*, 1–73.
(2) Hirose, K.; Goshima, Y.; Wakebe, T.; Tobe, Y.; Naemura, K. *Anal. Chem.* **2007**, *79*, 6295–6302.
(3) Aimi, J.; Oya, K.; Tsuda, A.; Aida, T. *Angew. Chem., Int. Ed.* **2007**, *46*, 2031–2035.
(4) Rekharsky, M. V.; Yamamura, H.; Inoue, C.; Kawai, M.; Osaka, I.; Arakawa, R.; Shiba, K.; Sato, A.; Ho, Y. H.; Selvapalam, N.; Kim, K.; Inoue, Y. *J. Am. Chem. Soc.* **2006**, *128*, 14871–14880.
(5) Scarso, A.; Rebek, J., Jr. *Supramol. Chirality* **2006**, *265*, 1–46.
(6) Iwasawa, T.; Hooley, R. J.; Rebek, J., Jr. *Science* **2007**, *317*, 493–496.
(7) Dong, V. M.; Fiedler, D.; Carl, B.; Bergman, R. G.; Raymond, K. N. *J. Am. Chem. Soc.* **2006**, *128*, 14464–14465.
(8) Ananchenko, G. S.; Pojarova, M.; Udachin, K. A.; Leek, D. M.; Coleman, A. W.; Ripmeester, J. A. *Chem. Commun.* **2006**, *4*, 386–388.
(9) Atwood, J. L.; Barbour, L. J.; Jerga, A. *J. Am. Chem. Soc.* **2002**, *124*, 2122–2123.
(10) Fiedler, D.; van Halbeek, H.; Bergman, R. G.; Raymond, K. N. *J. Am. Chem. Soc.* **2006**, *128*, 10240–10252.
(11) Kang, J. M.; Santamaria, J.; Hilmersson, G.; Rebek, J., Jr. *J. Am. Chem. Soc.* **1998**, *120*, 7389–7390.
(12) Pluth, M. D.; Bergman, R. G.; Raymond, K. N. *Science* **2007**, *316*, 85–88.
(13) Yoshizawa, M.; Tamura, M.; Fujita, M. *Science* **2006**, *312*, 251–254.
(14) Cerny, J.; Hobza, P. *Phys. Chem. Chem. Phys.* **2007**, *9*, 5291–5303.
(15) Meyer, E. A.; Castellano, R. K.; Diederich, F. *Angew. Chem., Int. Ed.* **2003**, *42*, 1210–1250.
(16) Houk, K. N.; Leach, A. G.; Kim, S. P.; Zhang, X. *Angew. Chem., Int. Ed.* **2003**, *42*, 4872–4897.
(17) Paulini, R.; Muller, K.; Diederich, F. *Angew. Chem., Int. Ed.* **2005**, *44*, 1788–1805.
(18) Mignon, P.; Loverix, S.; Steyaert, J.; Geerlings, P. *Nucl. Acids Res.* **2005**, *33*, 1779–1789.

10.1021/ic8012848 CCC: $40.75
Published on Web 11/20/2008

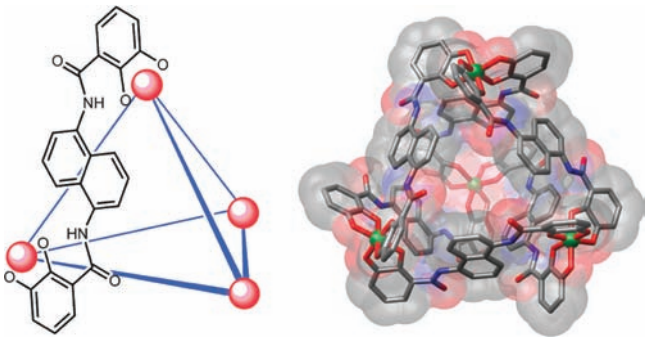

Figure 1. (Left) Schematic representation of the M_4L_6 assembly with only one ligand shown for clarity. (Right) A space-filling model of the assembly looking toward the aperture coincident with the 3-fold axis through which it is proposed that guests exchange.

time-average of such interactions is generally observed. However, solid-state structural analysis offers an opportunity to observe these forces in a static environment. Such studies have been instrumental in the identification and characterization of phenomena such cation$-\pi$ interactions or interactions between anions and electron-deficient aromatic rings in synthetic host molecules. While molecular modeling is often used to probe the basic structural properties of self-assembled systems, direct crystallographic analysis can often provide information about the size, shape, chirality, or geometric deformations in the system which would otherwise be unobtainable.

1.1. Background of the M_4L_6 Assembly. On the basis of rational design methods, Raymond and co-workers have explored the chemistry of synthetic supramolecular assemblies over the past decade. Assemblies of the stoichiometry M_4L_6 (M = Ga^{III}, Al^{III}, In^{III}, Fe^{III}, Ti^{IV}, or Ge^{IV}, L = N,N′-bis(2,3-dihydroxybenzoyl)-1,5-diaminonaphthalene) have been developed[19,20] and will be the focus of this structural study. The M_4L_6 assembly is a discrete, self-assembling tetrahedron in which the four metal ions define the vertices of the structure which are bridged by the six bis-bidentate ligands. The tris-bidentate coordination of the catechol amide moieties at the metal vertices makes each vertex a stereocenter and the rigid ligands transfer the chirality of one metal vertex to the others, thereby forming the homochiral ΔΔΔΔ or ΛΛΛΛ configurations.[21,22] While the 12− overall charge imparts water solubility for assemblies constructed from trivalent metal vertices, the interior cavity is defined by the naphthalene walls, thereby creating a hydrophobic environment that is isolated from the bulk aqueous solution. Although initial studies of the host−guest properties mainly provided information about the scope of guest encapsulation, the chemistry of the assembly has been expanded to include mechanistic studies of guest exchange,[23,24] mediation of reactivity,[25,26] and use as a catalyst.[10,12,27,28]

Although the solution behavior of **1** has been studied over the past decade, questions remain about the size, shape, and volume of the interior cavity of **1**, as well as how the exterior of the assembly is able to interact with guests. For example, empirical observations have shown that addition of an excess of π-acidic guests, such as Cp_2Co^+ or $Cp^*_2Co^+$ (Cp = η^5-cyclopentadienyl, Cp* = η^5-pentamethylcyclopentadienyl), to an aqueous solution of **1** results in precipitation of the assembly, suggesting that these cations are able to not only bind to the interior of **1**, but also to interact strongly with its exterior. In probing the ability of cations to ion-associate to the exterior of **1**, we have previously used pulsed gradient spin echo (PGSE) ^{1}H NMR methods to measure the diffusion coefficient of **1** in aqueous solution and have observed that hydrophobic cations, such as NEt_4^+ or NPr_4^+, are able to ion-associate to the exterior.[29] Similarly, we have obtained kinetic evidence for ion-association of hydrophobic tetraalkyl ammonium cations,[24] eneammonium cations,[10] and $Cp^*IrL_2X^+$ complexes[25] during mechanistic studies of guest exchange and reaction chemistry mediated by the assembly.

From studies of guest encapsulation, we know that the assembly is able to encapsulate guests as small as NMe_4^+ or as large as $Cp^*_2Co^+$. On the basis of the preference for filling empty cavities and the empirical observation by Rebek and co-workers that cavity-containing molecules tend to have 55% of their cavities filled by the encapsulated guest, we expect that the M_4L_6 assembly is able to distort to accommodate different guests.[30] In solution, the assembly generally exhibits *T*-symmetry (averaged on the NMR time scale), but upon encapsulation of $Cp^*_2Co^+$, the symmetry of the assembly is reduced to D_2.[24] This suggests that the guest is large enough to interact strongly with interior walls of **1,** which consequently prohibits fast tumbling of the guest inside the host. This raises the question of whether the inequivalence observed by ^{1}H NMR is caused by geometric or only magnetic inequivalence of the ligands.

The restricted size of the interior cavity of **1** has also been observed in reaction chemistry mediated by **1**. For the stoichiometric C−H bond activation of aldehydes by encapsulated $[Cp^*(PMe_3)Ir(Me)(\eta^2\text{-olefin})]^+$, small aldehydes are readily activated, whereas larger aldehydes, such as benzaldehyde, are too large to enter the assembly with the iridium compound already encapsulated.[25] Similarly, in the rhodium-catalyzed isomerization of allylic alcohols occurring inside of the $[Ga_4L_6]^{12-}$ assembly, size selectivity is extreme with only the two smallest substrates reacting in **1**.[26] The same

(19) Caulder, D. L.; Powers, R. E.; Parac, T. N.; Raymond, K. N. *Angew. Chem., Int. Ed.* **1998**, *37*, 1840–1843.
(20) Caulder, D. L.; Raymond, K. N. *Acc. Chem. Res.* **1999**, *32*, 975–982.
(21) Davis, A. V.; Fiedler, D.; Ziegler, M.; Terpin, A.; Raymond, K. N. *J. Am. Chem. Soc.* **2007**, *129*, 15354–15363.
(22) Terpin, A. J.; Ziegler, M.; Johnson, D. W.; Raymond, K. N. *Angew. Chem., Int. Ed.* **2001**, *40*, 157–160.
(23) Davis, A. V.; Fiedler, D.; Seeber, G.; Zahl, A.; van Eldik, R.; Raymond, K. N. *J. Am. Chem. Soc.* **2006**, *128*, 1324–1333.
(24) Davis, A. V.; Raymond, K. N. *J. Am. Chem. Soc.* **2005**, *127*, 7912–7919.
(25) Leung, D. H.; Bergman, R. G.; Raymond, K. N. *J. Am. Chem. Soc.* **2006**, *128*, 9781–9797.
(26) Leung, D. H.; Bergman, R. G.; Raymond, K. N. *J. Am. Chem. Soc.* **2007**, *129*, 2746–2747.
(27) Fiedler, D.; Bergman, R. G.; Raymond, K. N. *Angew. Chem., Int. Ed.* **2004**, *43*, 6748–6751.
(28) Pluth, M. D.; Bergman, R. G.; Raymond, K. N. *Angew. Chem., Int. Ed.* **2007**, *46*, 8587–8589.
(29) Pluth, M. D.; Tiedemann, B. E. F.; van Halbeek, H.; Nunlist, R.; Raymond, K. N. *Inorg. Chem.* **2008**, *47*, 1411–1413.
(30) Mecozzi, S.; Rebek, J., Jr. *Chem.—Eur. J.* **1998**, *4*, 1016–1022.

types of size selectivities have been observed when using the assembly as a catalyst for the hydrolysis of acid-sensitive substrates.[12,28] In the hydrolysis of orthoformates, only substrates smaller than tri-*n*-pentyl orthoformate are able to enter the assembly to undergo hydrolysis. Similarly, for the hydrolysis of acetals, small acetals are readily hydrolyzed inside of the assembly, whereas larger acetals are not. These data suggest an upper size limit to guests permitted entry into the interior cavity of the assembly, a limit that could be lower than the full volume of the cavity itself (vide infra).

In addition to the size of the assembly, the shape of the interior cavity has been important in previous host−guest chemistry. Although the chirality of the assembly is generated at each of the metal vertices, it can be transferred to the encapsulated guests and has been used for diastereoselective encapsulation of substrates such as ruthenium half-sandwich complexes[31] and the diastereoselective reactivity of encapsulated iridium complexes.[25] For both of these cases, the diastereoselectivities observed in the $[Ga_4L_6]^{12-}$ assembly are lowest for either very small or very large guests, with the optimal selectivities being obtained with guests of intermediate size. By analyzing the interior cavity shapes and volumes, as well as the effect of charge on the cluster properties, from the molecular structure data, we hoped to learn more about the origin of this selectivity.

2. Results and Discussion

2.1. Synthesis of Host−Guest Complexes for Crystallographic Analysis. The host−guest complex $(NEt_4)_7[NEt_4 \subset Ti_4L_6]$ (**3**) (where $\subset$ denotes encapsulation) was prepared from the correct stoichiometry of H_4L, $Ti(O^iPr)_4$, and NEt_4Cl in refluxing DMF as previously described.[24] The ^{1}H NMR spectrum confirms formation of an octa-anionic *T*-symmetric species associated with 1 equiv of encapsulated NEt_4^+ and 7 equiv of exterior NEt_4^+. Crystals suitable for X-ray diffraction were grown by diffusing methanol into a DMF solution of the bulk material. The complex crystallizes in the space group $R\bar{3}c$ with 12 molecules in the unit cell.

The host−guest complex $(BnNMe_3)_{11}[BnNMe_3 \subset Ga_4L_6]$, Bn = CH_2Ph] (**4**) was prepared from the H_4L ligand and $Ga(acac)_3$ using $BnNMe_3OH$ as the base. The ^{1}H NMR spectrum shows two different $BnNMe_3^+$ resonances in a ratio of 11:1 corresponding to the exterior and encapsulated guest molecules. Crystals suitable for X-ray diffraction studies were obtained by diffusing acetone into a wet DMF/DMSO solution of the complex. The complex crystallizes in the space group $P2_1/n$ with four molecules per unit cell.

The host−guest complex $(NMe_2H_2)_{5.5}(Cp_2Co)_{1.5}[Cp_2Co \subset Ti_4L_6]$ (**5**) was prepared from the H_4L ligand, $Ti(O^iPr)_4$, and 3 equiv of $[Cp_2Co][PF_6]$ in refluxing DMF. The decomposition of DMF provided the base required to deprotonate H_4L. Crystals suitable for X-ray diffraction were obtained by diffusing methanol into a wet DMF solution of the complex. The complex crystallizes with 2.5 equivalents of Cp_2Co^+ per Ti_4L_6 in the space group $R\bar{3}c$ with twelve molecules in each unit cell.

(31) Fiedler, D.; Leung, D. H.; Bergman, R. G.; Raymond, K. N. *J. Am. Chem. Soc.* **2004**, *126*, 3674–3675.

The host−guest complex $K_8(Cp^*_2Co)_3[Cp^*_2Co \subset Ga_4L_6]$ (**6**) was prepared from the H_4L ligand, $Ga(acac)_3$, and 4 equiv of $[Cp^*_2Co][PF_6]$ in MeOH using KOH as the base. Crystals suitable for X-ray diffraction studies were obtained by diffusing acetone into a 5:1 solution of DMSO/MeOH. The complex crystallizes with 3 equiv of $Cp^*_2Co^+$ per Ga_4L_6 in the space group $Fd\bar{3}c$ with sixteen molecules in each unit cell.

2.2. Structural Analysis. Despite the breadth of chemistry reported for M_4L_6 assemblies, only two molecular structures have been reported to date because of the difficulty of growing crystals suitable for X-ray diffraction studies. The first X-ray structure of the M_4L_6 assembly was that determined for the complex $K_5(NEt_4)_6[NEt_4 \subset Fe_4L_6]$ (**1**), which crystallizes in the space group $I\bar{4}3d$ with 16 molecules in each unit cell (CCDC-100947).[19] The second published structure was the enantiopure $\Delta,\Delta,\Delta,\Delta$-$(NEt_4)_{11}[NEt_4 \subset Ga_4L_6]$ (**2**), which crystallizes in the space group $I23$ with 2 molecules in the unit cell (CCDC-145431).[22] One challenge in crystallizing these highly charged, highly symmetric molecules is the need to efficiently pack unencapsulated counterions in the crystal lattice. Depending on the charge of the metal vertices, the M_4L_6 assembly either has a 12− or 8− overall charge, which, when one monocationic guest is encapsulated, leaves either 11 or 7 countercations, respectively; these are difficult to efficiently pack in a high symmetry environment.

2.2.1. Analysis of 3. Comparison of the structure of $(NEt_4)_7[NEt_4 \subset Ti_4L_6]$ (**3**) with the $(NEt_4)_{11}[NEt_4 \subset M_4L_6]$ structures of **1** (M = Fe^{III}) and **2** (M = Ga^{III}) can be used to probe the effect of metal ion on the resulting assembly structure. In the structure of **3** in $R\bar{3}c$ (Figure 2), one of the titanium atoms in the assembly and the nitrogen of the encapsulated NEt_4^+ lie on the 3-fold axis (Wycoff position *c*) with the other three titanium atoms of the assembly lying on general positions. The Ti_4L_6 assembly has 3-fold crystallographic symmetry, with the encapsulated guest disordered about the 3-fold axis. The crystallographic disorder of this cation was modeled with one of the methyl group carbon atoms also lying on the 3-fold axis with the adjacent methylene group disordered over three positions. Of the exterior cations, one molecule of NEt_4^+ is crystallographically ordered in the asymmetric unit with pseudo-S_4 symmetry and is located near the catechol rings of the assembly. A second NEt_4^+ cation is located near the 3-fold aperture of the assembly and is disordered. (See the Supporting Information for an expanded discussion of the disorder modeling.)

2.2.2. Analysis of 4. Crystallographic analysis of the host−guest complex containing both encapsulated and exterior $BnNMe_3^+$ enabled investigation of how cations capable of both $\pi-\pi$ and cation$-\pi$ interactions associate with the assembly. This structure crystallizes in the lowest symmetry space group of any of the known structures of the M_4L_6 assembly ($P2_1/n$), with the favorable consequence that all of the $BnNMe_3^+$ cations are crystallographically ordered (Figure 3). Here in the solid state a lower symmetry guest with significant noncovalent host-guest interactions

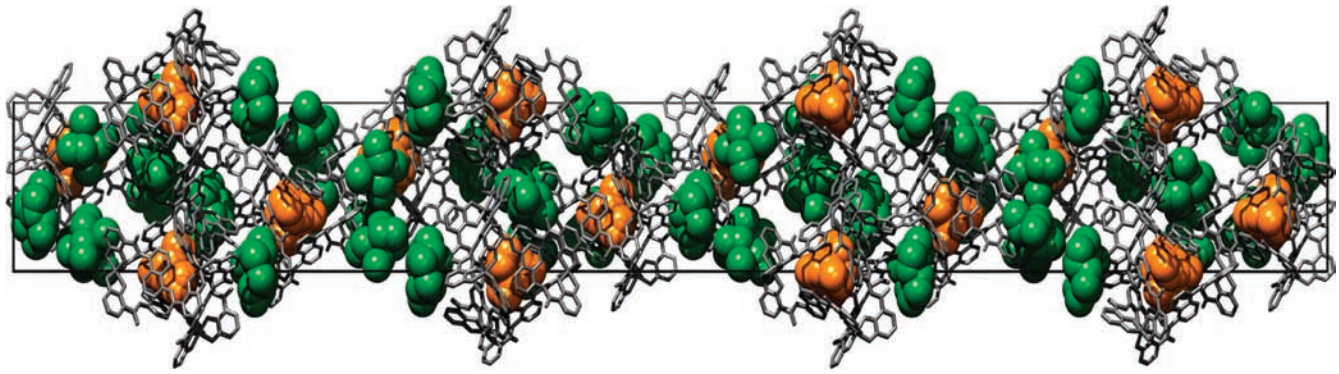

Figure 2. Unit cell diagram for **3** looking down the *b* axis. Hydrogen atoms and solvent have been removed for clarity. The different components of the unit cell have been color coded: host molecule (gray), encapsulated guests (orange), exterior guests (green).

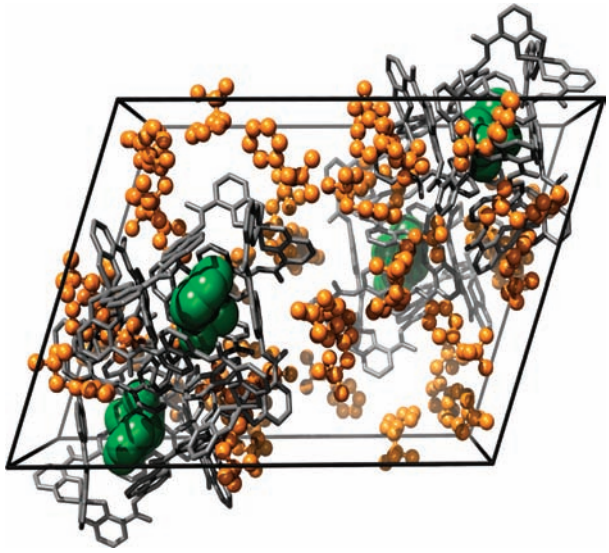

Figure 3. Unit cell diagram for **4**. Hydrogen atoms and solvent molecules have been removed for clarity. Different components of the unit cell have been color coded: host molecule (gray), encapsulated guests (orange), and exterior guests (green).

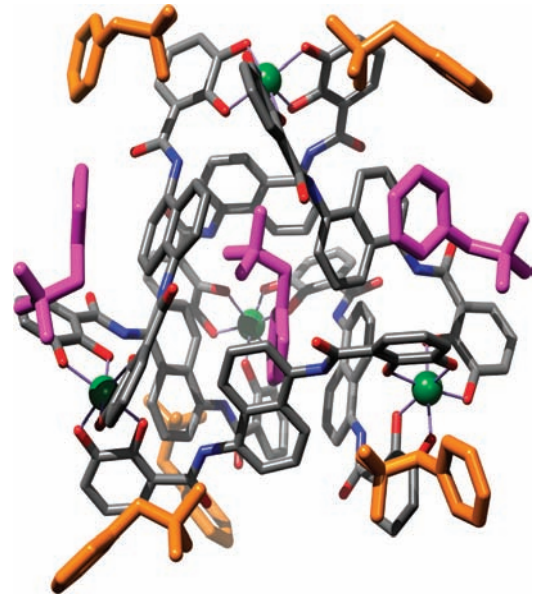

Figure 4. Diagram showing interactions of NMe_3Bn^+ molecules with the host assembly in **4**. For clarity, different components of the assembly have been color coded: carbon (gray), nitrogen (blue), oxygen (red), and gallium (green). The $BnNMe_3^+$ cations have been color coded based on how they interact with the assembly: $\pi-\pi$ interactions (purple) and cation$-\pi$ interaction (orange).

lowers the symmetry of the host and of the crystal lattice. The cluster itself does not have crystallographic symmetry; the Ga−Ga distances range from 12.56 to 12.89 Å and average 12.7(1) Å.

The encapsulated $BnNMe_3^+$ cation interacts with the interior walls of the assembly with both $\pi-\pi$ and cation$-\pi$ interactions. The phenyl ring of the encapsulated $BnNMe_3^+$ has a closest contact from the center of the benzene ring to a naphthalene carbon atom of 3.63 Å and an interplanar angle between the least-squares plane of the phenyl ring and the naphthalene ring of 14.4°. The face of the naphthalene ring of the assembly opposite to the interacting encapsulated $BnNMe_3^+$ does not interact with any of the cations on the exterior of the assembly. The NMe_3^+ moiety of the $BnNMe_3^+$ guest is oriented toward the three adjacent catechol rings at the vertex of the assembly with a closest contact of 3.75 Å.

The eleven remaining $BnNMe_3^+$ cations pack around the exterior of the assembly, with some of the cations interacting with the exterior of the assembly by either $\pi-\pi$ or cation$-\pi$ interactions. All of the $\pi-\pi$ interactions to the exterior of the assembly occur between the naphthalene rings and the phenyl ring of the cation (with distances between the phenyl centroid of the $BnNMe_3^+$ and the least-squares plane of the naphthalene of 3.95 and 3.62 Å and interplanar angles between the least-squares planes of the phenyl ring and naphthalene of 28.1° and 12.6°, respectively). The NMe_3^+ moiety of the $BnNMe_3^+$ cation interacts with the exterior of the assembly through cation$-\pi$ interactions and fits into the wedges created by adjacent electron-rich catecholate rings near the vertices of the assembly (Figure 4). None of the exterior cations bridge adjacent assemblies in the crystal.

2.2.4. Analysis of 5. The structure of $(NMe_2H_2)_{5.5}(Cp_2Co)_{1.5}[Cp_2Co \subset Ti_4L_6]$ (**5**) demonstrates that two assemblies can be bridged through $\pi-\pi$ overlap between the parallel but opposite cyclopentadienyl rings of the Cp_2Co^+ and the naphthalene walls of the assembly. Similar to the structure of **3** (the other Ti(IV)-derived structure), **5** crystallizes in $R\bar{3}c$ (Figure 5). One of the titanium atoms from each cluster, as well as the cobalt atom of the encapsulated Cp_2Co^+, lies on the crystallographic 3-fold axis (Wycoff position *c*) with the other titanium atoms of the host lying on general positions. The 3-fold crystallographic axis runs

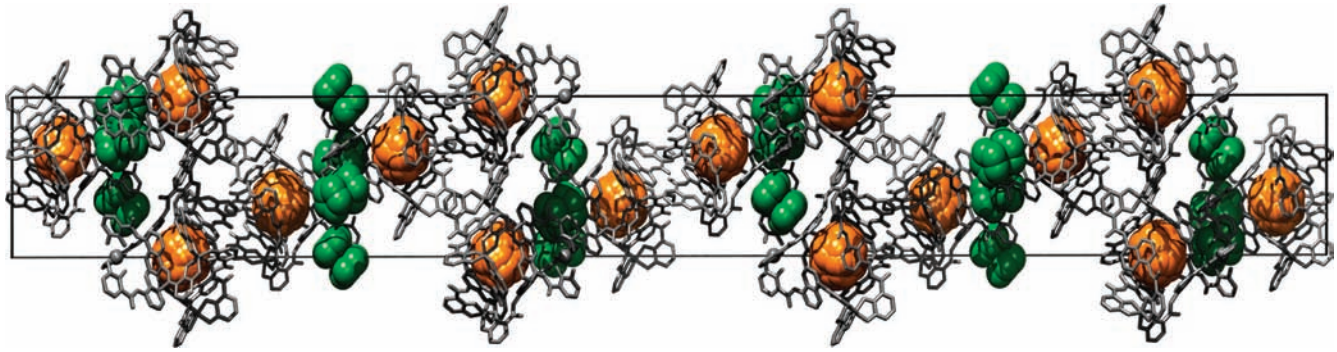

Figure 5. Unit cell diagram for **5** looking down the *b* axis. Hydrogen atoms, dimethylammonium counterions, and solvent have been removed for clarity. The different components of the unit cell have been color coded: host molecule (gray), encapsulated guests (orange), and exterior guests (green).

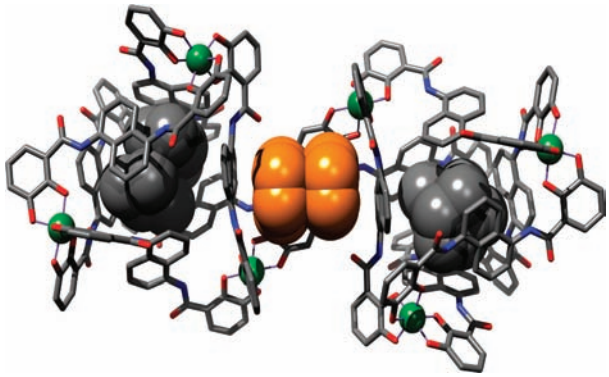

Figure 6. Diagram showing a Cp_2Co^+ molecule bridging two host molecules by parallel but opposite π-stacking. For clarity, different components of the unit cell have been color coded: carbon (gray), nitrogen (blue), oxygen (red), gallium (green), encapsulated guests (gray), and exterior guest (orange).

through the guest with a cyclopentadienyl ring centroid−Co-Ti angle of 65°. The atoms of the cyclopentadienyl ring were modeled from a known structure[32] of Cp_2Co^+ and are disordered to conform to the local site symmetry. The exterior Cp_2Co^+ sits at a position with 2-fold site symmetry (Wycoff position *e*) and is ordered in the crystal lattice, with local D_{5d} symmetry. Because of the the elongated thermal ellipsoids of carbon atoms on the cyclopentadienyl rings, the exterior Cp_2Co^+ was similarly modeled to the known structure of Cp_2Co^+.

If one looks beyond the asymmetric unit of **5**, the role of the exterior 1.5 Cp_2Co^+ ions per tetrahedron becomes apparent. The exterior Cp_2Co^+ π-stacks between adjacent assemblies with a distance of 3.38 Å between the cyclopentadienyl ring of the Cp_2Co^+ and the least-squares plane of the naphthalene ring of the assembly, with an interplanar angle between the cyclopentadienyl and naphthalene rings of 4.7° (Figure 6). Each assembly in the crystal lattice interacts with three bridging Cp_2Co^+ molecules, leading to the formation of groups of four Ti_4L_6 assemblies and three external Cp_2Co^+ molecules throughout the crystal lattice (Figure 7). The C−H bonds of the exterior Cp_2Co^+ are also in close proximity to the electron-rich catechol rings of the assembly, with a distance of 2.8 Å between the C−H bond and the least-squares plane of the catechol ring (or 2.9 Å between the C−H bond and the centroid of the catechol ring), which is consistent with CH−π interactions.

(32) Braga, D.; Grepioni, F. *Chem. Commun.* **1998**, *8*, 911–912.

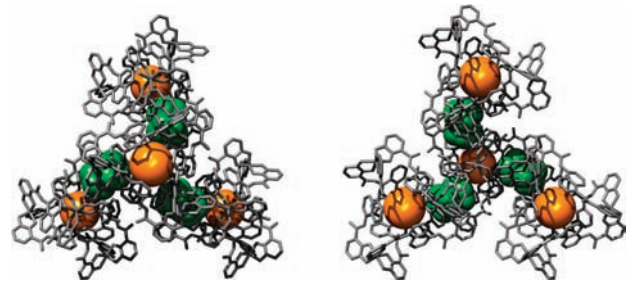

Figure 7. Diagram showing the interaction of the Cp_2Co^+ with adjacent clusters in the unit cell. For clarity the encapsulated Cp_2Co^+ is shown as a sphere (orange) and different components of the unit cell have been color coded: assembly (gray) and exterior guest (green).

2.2.4. Analysis of 6. Inspired by the crystallographic features of **5**, the more sterically demanding $Cp^*_2Co^+$ was explored in $K_9(Cp^*_2Co)_2[Cp^*_2Co \subset Ga_4L_6]$ (**6**). The host−guest complex crystallizes in the space group $Fd\bar{3}c$ such that the assembly has its full *T* point group symmetry (Wycoff position *a*) and the encapsulated $Cp^*_2Co^+$ guest is disordered at the center of the assembly with this same symmetry and has an interplanar least-squares plane angle of 3.9° relative to that of the naphthalene ring of the assembly (Figure 8). The exterior $Cp^*_2Co^+$ lies on a special position with $\bar{3}$ symmetry (Wycoff position *c*). Both $Cp^*_2Co^+$ molecules were modeled from a known structure of $Cp^*_2Co^+$ and are disordered based on the local site symmetry. Their constrained refinement with these disorder models are described in the Supporting Information. The exterior K^+ atoms lie on the *d*-glide and are disordered over three positions around the vertex of each assembly. The overall lattice has large solvent channels which lack long-range crystallographic order.

Stoichiometry requires two exterior $Cp^*_2Co^+$ ions per assembly; each of these cations lies near the 3-fold aperture of the assembly (Figure 9), and they bridge adjacent assemblies throughout the lattice. The Cp* rings are likely too sterically demanding to π-stack with the naphthalene units as was observed in the structure of **5**. The located K^+ cations are near the catechol oxygen of the cluster and interact with catechol oxygens of adjacent assemblies. On the basis of the disorder and partial occupancy of the K^+

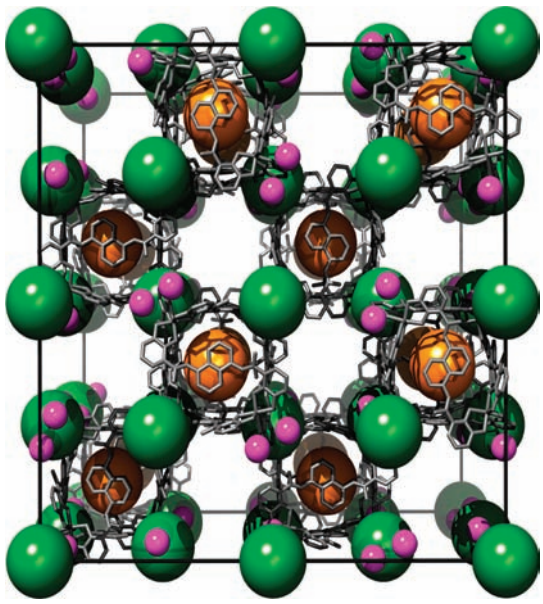

Figure 8. Unit cell diagram for **6**. For clarity, hydrogen atoms and solvent molecules have been removed. Disordered $Cp^*_2Co^+$ are represented as spheres and different components of the unit cell have been color coded: host molecules (gray), potassium (purple), encapsulated guests (orange), and exterior guests (green).

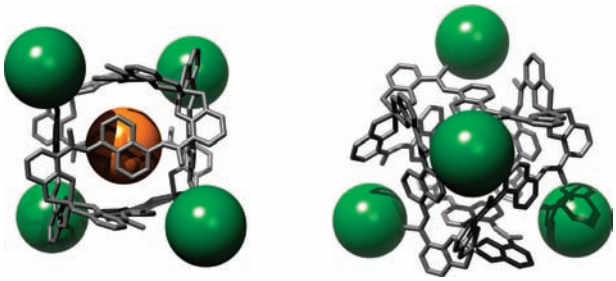

Figure 9. Interactions between disordered $Cp^*_2Co^+$ cations and the host molecules. Left: Viewed down the 2-fold axis. Right: Viewed down the 3-fold axis. For clarity, $Cp^*_2Co^+$ molecules are represented as spheres and the components have been color coded: host molecule (gray), encapsulated guest (orange), and exterior guest (green).

cations, each vertex of the assembly shares one potassium atom with the adjacent assembly.

2.3. Structural Comparison. The four molecular structures described above (**3**−**6**), as well as the two previously published crystal structures (**1**−**2**), were compared to examine how the assembly is able to accommodate differently sized guests and the structural effect of replacing the trivalent metal vertices with tetravalent Ti^{IV} ions. The assembly metrical parameters from the six M_4L_6 structures are compared in Tables 2 and 3. The root-mean-square distances (rmsd) between each of the atoms of the assembly were calculated to compare the six structures pairwise.[33] As expected, the three NEt_4^+ structure are the most similar, with rmsd values ranging from 0.459 to 0.478 Å. In each case, the differences in the twist of the naphthalene rings accounted for the majority of the distance between structures being compared.

In a further comparison of the six structures, the average metal−metal distances were compared; they show little deviation. In the structure of **3**, the Ti−Ti distances average 12.75 Å, similar to the 12.78 Å Fe−Fe and the 12.66 Å Ga−Ga distances in **1** and **2**, respectively. The small differences are likely the result of the difference in the overall charge of the assembly molecules and variations in packing of each structure.

The shortest M−M distance is 12.60 Å for **6**. This shorter M−M distance allows the naphthalene ligands to bow outward slightly to help accommodate the sterically demanding $Cp^*_2Co^+$ guest. This is illustrated by comparison of the average distance between opposing naphthalene centroids. The maximum of this metric is also found in structure **6**, with a naphthalene−naphthalene distance that is 0.72 Å larger than the next largest distance of 10.42 Å in the case of **3**. It might be expected that the short M−M distance of **6** would be caused by greater twisting of the catecholate metal centers, and the twist angle (θ, as defined by Kepert[35,36]) for each structure was calculated for the metal vertex coincident with the crystallographic 3-fold axis. Notably, the largest twist angles (24.8° and 25.9° for structures **2** and **6**, respectively) correspond to the shortest M−M distances. However, the average twist angle for the four metal centers of one structure does not correlate with M−M distance, demonstrating that these structural changes reflect the sum of many small distortions of the ligands and metal complexes of the structure.

One measure of the malleability of the host is the observed variation in the cavity width as defined by the distance between the centroids of opposite naphthalene walls. From the Cp_2Co^+ encapsulating structure (**5**) the average cavity width can expand a full angstrom in order to accommodate $Cp^*_2Co^+$. Similarly, the shape of the cavity can be greatly influenced by the angles between the mean planes of the opposing naphthalene walls. This angle varies greatly: from 47° in the case of **1** to 0° for **6**. A large naphthalene−naphthalene angle should help to transfer the chirality from the metal vertices to the interior cavity of the assembly. In addition, the distance from the center of the assembly to the centroids of the catechol rings gives a measure of how much the ligands have bowed out.

To further analyze the cavities of the host−guest complexes, the void spaces were modeled using the computer program *Voidoo*,[37−39] which maps out the interior of the cavity using a 1.4 Å radius rolling probe. This method uses the van der Waals radii of atoms to generate a solvent-accessible surface corresponding to the cavity of the host molecule. From the analysis of the void spaces, a number of observations can be made. First, the metal vertices are inaccessible to the guest molecules, suggesting that the chirality at the metal centers cannot be directly transmitted

(33) For the RMSD comarisons, the guest molecules were excluded, as well as the hydrogen atoms of the assembly.

(34) Structures were aligned along their respective crystallographic 3-fold axes. For structural comparisons with multiple rmsd settings caused by symmetry, the minimum rmsd is reported in the table. The average rmsd values of different settings are **1/4**, 0.741; **2/4**, 0.691; **3/4**, 0.631; **4/5**, 0.641.

(35) Kepert, D. L. *Inorg. Chem.* **1972**, *11*, 1561–1563.
(36) Kepert, D. L. *Prog. Inorg. Chem.* **1977**, *23*, 1–65.
(37) Kleywegt, G. J.; Jones, T. A. *Acta Crystallogr.* **1994**, *D50*, 178–185.
(38) Kleywegt, G. J.; Zou, J. Y.; Kjeldgaard, M.; Jones, T. A. *International Tables for Crystallography*; International Union of Crystallography, Kluwer Academic: Dordrecht, The Netherlands, 2001; Volume *F*, Chapter 17.1, pp. 353−356, 366−367.

Table 1. Crystal Data for Complexes **3**−**6**

	3	**4**	**5**	**6**
formula	$C_{182}H_{111}N_{17.5}O_{36}Ti_4$	$C_{293}H_{265}Ga_4N_{27.5}O_{41.5}$	$C_{100.75}H_{96}Co_{2.5}N_{16}O_{56.6}Ti_4$	$C_{204}H_{174}Co_3Ga_4K_9N_{12}O_{36}$
mol wt	3310.48	5144.21	3722.60	4177.12
cryst appearance	trigonal prism	rectangular prism	plate	cube
cryst color	orange	orange	red	yellow
cryst syst	trigonal	trigonal	monoclinic	cubic
space group	$R\bar{3}c$ (No. 167)	$P2_1/n$ (No. 14)	$R\bar{3}c$ (No. 167)	$Fd\bar{3}c$ (No. 228)
a [Å]	20.844(3)	26.7393(6)	20.5378(7)	50.0040(21)
b [Å]	20.844(3)	30.8317(2)	20.5378(7)	50.0040(21)
c [Å]	163.55(5)	38.5228(8)	169.966(11)	50.0040(21)
α [deg]	90.00	90.00	90.00	90.00
β [deg]	90.00	109.853(1)	90.00	90.00
γ [deg]	120.00	90.00	120.00	90.00
Z	12	4	12	16
V [Å^3]	61 540(25)	29 871.4(9)	620 867(5)	125 030(9)
ρ [g cm^{-3}]	1.072	1.137	1.120	0.888
μ [mm^{-1}]	0.27	0.43	0.42	0.89
cryst size [mm^3]	0.16 × 1.12 × 0.12	0.48 × 0.25 × 0.18	0.33 × 0.19 × 0.12	0.30 × 0.30 × 0.30
temp (K)	173(2)	293(2)	178(2)	173(2)
λ (Å)	0.77490	0.71073	0.71073	0.77490
F(000)	20418	10686	22724	34336
θ max [deg]	19.3	19.8	17.3	22.8
limiting indices	$-17 < h < 17$	$-24 < h < 22$	$-17 < h < 9$	$-45 < h < 46$
	$-17 < k < 17$	$-16 < k < 29$	$-15 < k < 17$	$-49 < k < 38$
	$-133 < l < 138$	$-36 < l < 36$	$-141 < l < 141$	$-45 < l < 49$
measured reflns	48435	71416	42016	73270
independent reflns	4345	26371	4201	2738
reflns ($I < 2\sigma(I)$)	3636	14 441	2811	1091
params	426	1634	440	177
restraints	564	68	275	145
data/param ratio	10.2	16.1	9.6	15.5
R^a ($I < 2\sigma(I)$)	0.154	0.128	0.157	0.146
wR^b ($I < 2\sigma(I)$)	0.453	0.316	0.425	0.366
R^a (all data)	0.170	0.205	0.192	0.224
wR^b (all data)	0.467	0.410	0.448	0.407
GOF	2.16	1.04	1.84	1.20
$\Delta\rho_{max}$ [e/Å^3]	+0.73	+1.16	+0.94	+0.61
$\Delta\rho_{min}$ [e/Å^3]	−0.73	−1.61	−0.53	−0.41

[a] R factor definition: $R = \Sigma(||F_o| - |F_c||)/\Sigma|F_o|$. [b] SHELX-97 wR factor definition: $wR = [\Sigma w(F_o^2 - F_c^2)^2/\Sigma w(F_o^2)]^{1/2}$. Weighting scheme: $w = 1/[\sigma^2(F_o)^2 + (np)^2]$, $p = [F_o^2 + 2F_c^2]/3$.

Table 2. Comparison of the Root Mean Square Distances (rmsd) between Structures **1**−**6**[34]

	rmsd (Å)				
	2	**3**	**4**	**5**	**6**
1	0.464	0.478	0.662	0.659	0.670
2		0.459	0.577	0.619	0.503
3			0.609	0.646	0.576
4				0.571	0.544
5					0.546

Table 3. Comparison of Structural Parameters of Structures **1**−**6**

	1	**2**	**3**	**4**	**5**	**6**
space group	$I\bar{4}3d$	$I23$	$R\bar{3}c$	$P2_1/n$	$R\bar{3}c$	$Fd\bar{3}c$
assembly symmetry[a]	C_3	C_3	C_3	C_1	C_3	T
M−M distance (Å)[b]	12.78	12.66	12.79	12.81	12.79	12.60
naphthalene−naphthalene (Å)[c]	10.30	10.41	10.42	10.38	10.13	11.14
naphthalene−naphthalene (deg)[d]	47.20	[g]	41.04	41.61	20.88	0.00
center−metal (Å)[e]	7.74	8.03	7.82	7.84	7.81	7.71
twist angle (θ) from C_3 (deg)[f]	20.2	24.8	19.8	-	16.8	25.9
average twist angle (θ_{avg}) (deg)	18.4	20.2	21.4	24.2	20.0	20.4

[a] Point symmetry of the assembly. [b] Taken as the average for noncubic structures. [c] Average between the centroids of opposing naphthalene rings. [d] Average between the planes of opposing naphthalene rings. [e] Measured from the centroid of the metal vertices to each metal. [f] Measured for metal vertex with crystallographic 3-fold symmetry. [g] Disorder of the naphthalene rings prohibited determination of an accurate least-squares plane.

to the encapsulated guests. This observation is also consistent with previous solution 2D ^{1}H NOESY experiments, which show strong through-space interactions between the guest and the naphthalene rather than catechol hydrogens.[25,40] Second, the shape of the void cavity varies greatly with guest, with the shape being primarily defined by the naphthalene rings rather than the catechol moieties. The angle between opposing naphthalene walls has a large influence on the shape of the cavity surface. In addition, the largest guest, $Cp^*_2Co^+$, greatly deforms the shape of the interior cavity, so that it resembles a cube. These observations help to explain the diastereoselectivities observed for the M_4L_6 structure. If the guest is too small, the steric interactions with the assembly are too small to efficiently transfer the chirality of the assembly to the encapsulated guest. Conversely, if the guest is too large, distortion of the interior cavity to a pseudocubic void greatly diminishes the chiral induction generated by the angle between opposing naphthalene walls of the assembly ligands. The solvent accessible shapes are shown in Figure 10 (videos of the void spaces are available in the Supporting Information).

To examine how efficiently the guests pack inside the host assembly, the packing coefficients for each host−guest

(39) Molecular graphics images were produced using the UCSF Chimera package from the Resource for Biocomputing, Visualization, and Informatics at the University of California, San Francisco (supported by NIH P41 RR-01081). Pettersen. E. F.; Goddard, T. D.; Huang, C. C.; Couch, G. S.; Greenblatt, D. M.; Meng, E. C.; Ferrin, T. E. *J. Comput. Chem.* **2004**, *25*, 1605–1612.

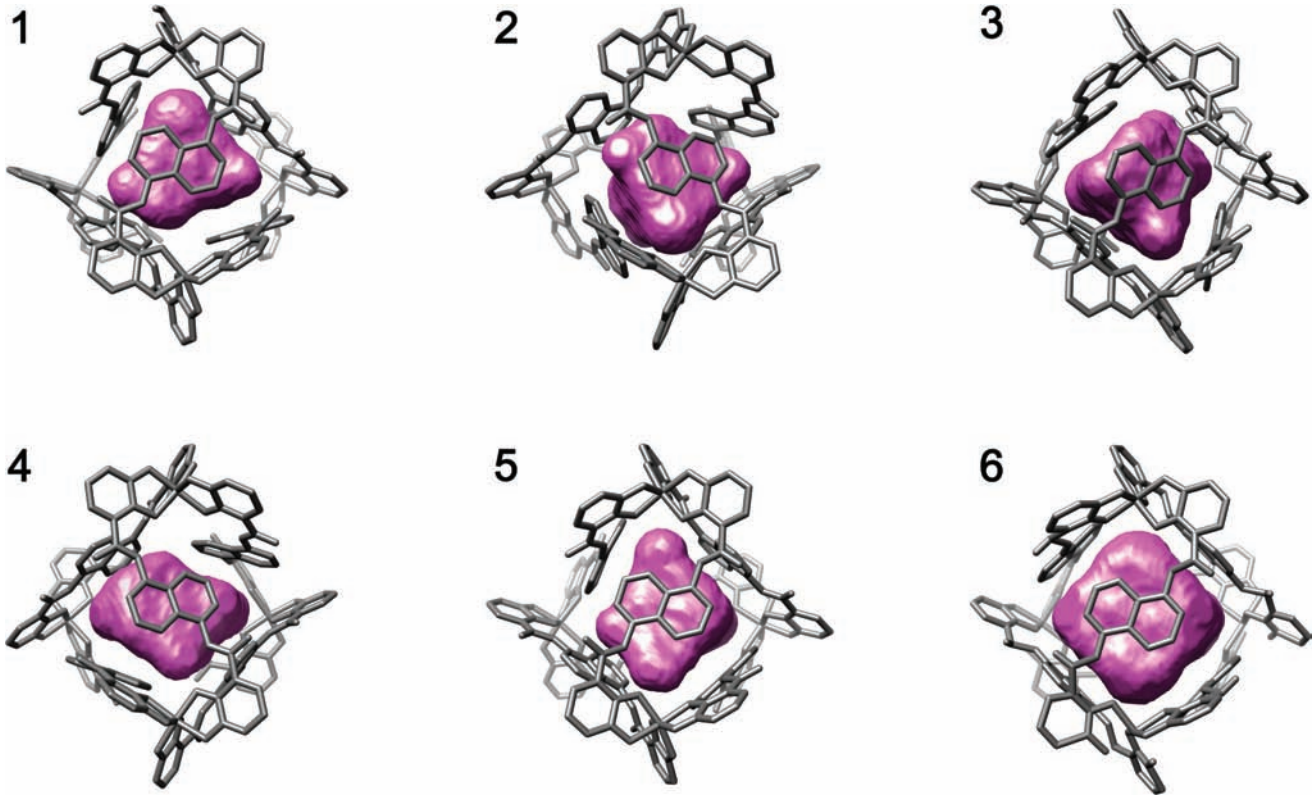

Figure 10. Depiction of the solvent accessible (1.4 Å rolling probe) void cavities of each of the crystal structures. Hydrogen atoms and all exterior molecules are excluded for clarity.

complex were determined. The packing coefficient is defined as the volume of the encapsulated guest (or guests) divided by the solvent accessible volume of the interior cavity, as shown in eq 1. A number of studies have investigated the packing coefficient in either calculated, synthetic, or biological host−guest structures and found that an ideal packing coefficient is 0.55 ± 0.09.[30,41−45] Deviation from the 0.55 ideal generally results from other forces between either the encapsulated guest and host or between exterior molecules and the host.

$$\mathrm{PC} = \frac{\sum_{i=1}^{n} v_w^i}{V_{\mathrm{cav}}} = \frac{V_w}{V_{\mathrm{cav}}} \qquad (1)$$

The packing coefficients of the structures **1** and **2** of 0.53 and 0.55, respectively, show the optimal packing of the encapsulated NEt_4^+ cation (Table 4). For the other NEt_4^+-containing structure, **3**, the volume of the interior cavity of the assembly is larger than in either **1** or **2**, which leads to a lower packing coefficient. It is likely that these differences arise from crystal packing forces, since compounds **1**−**3** all crystallize in different space groups. The structure of **4** also shows an ideal packing coefficient of 0.54. The two host−guest complexes containing metallocene guests, **5** and **6**, have packing coefficients of 0.54 and 0.67, respectively. Remarkably, despite the strong $\pi-\pi$ exterior interactions in **4** and **5**, the packing coefficients remain 0.54. For structure **6**, containing the largest guest, $Cp^*_2Co^+$, the packing coefficient is significantly higher than the 0.55 ideal, suggesting that the host molecule is not able to distort enough to ideally accommodate the $Cp^*_2Co^+$ guest. This finding supports the constrictive binding observed in solution for $[Cp^*_2Co \subset Ga_4L_6]^{11-}$ as evidenced by its slow guest exchange behavior.[24]

Table 4. Cavity Volumes, Guest Volumes, and Packing Coefficients for the Host−Guest Complexes

	volume (Å^3)		
structure	cavity	guest	PC
1	261	138	0.53
2	253	138	0.55
3	293	138	0.47
4	285	153	0.54
5	270	145	0.54
6	434	291	0.67

3. Conclusion

In summary, we have used X-ray crystallographic analysis to probe host−guest interactions in the highly charged, self-assembled M_4L_6 supramolecular cluster. Depending on the encapsulated guest, we see that intermolecular forces such

(40) Pluth, M. D.; Bergman, R. G.; Raymond, K. N. *J. Am. Chem. Soc.* **2007**, *129*, 11459–11467.
(41) Zürcher, M.; Gottschalk, T.; Meyer, S.; Bur, D.; Diederich, F. *ChemMedChem* **2008**, *3*, 237–240.
(42) Rekharsky, M. V.; Mori, T.; Yang, C.; Ko, Y. H.; Selvapalam, N.; Kim, H.; Sobransingh, D.; Kaifer, A. E.; Liu, S.; Isaacs, L.; Chen, W.; Moghaddam, S.; Gilson, M. K.; Kim, K.; Inoue, Y. *Proc. Nat. Acad. Sci. U.S.A.* **2007**, *104*, 20737–20742.
(43) Ajami, D.; Rebek, J., Jr. *Proc. Nat. Acad. Sci. U.S.A.* **2007**, *104*, 16000–16003.
(44) Fogarty, H. A.; Berthault, P.; Brotin, T.; Huber, G.; Desvaux, H.; Dutasta, J. P. *J. Am. Chem. Soc.* **2007**, *129*, 10332–10333.
(45) Watabe, T.; Kobayashi, K.; Hisaki, I.; Tohnai, N.; Miyata, M. *Bull. Chem. Soc. Jpn.* **2007**, *80*, 464–475.

as $\pi-\pi$, cation$-\pi$, and CH$-\pi$ interactions influence the binding and orientation of the encapsulated guests. Cation$-\pi$ interactions appear to be localized near the electron-rich catechol rings of the assembly, and $\pi-\pi$ interactions are localized near the naphthalene walls. Changing the metal and its charge at the vertex does not have a significant effect on the geometry or shape of the host assembly. In contrast, the interior cavity of the assembly is able to distort to accommodate a wide variety of guest molecules with the shape of the internal cavity being primarily defined by the naphthalene walls of the assembly. The volume of the internal solvent-accessible cavity of the assembly ranges between 253 and 434 Å^3, depending on the encapsulated guest.

4. Experimental Section

4.1. General. 4.1.1. General Procedures. All NMR spectra were obtained using Bruker AV-400 or AV-500 MHz spectrometers at the indicated frequencies. Chemical shifts are reported as parts per million (δ) and referenced to residual protic solvent peaks. The following abbreviations are used in describing NMR couplings: (s) singlet, (d) doublet, (t) triplet, (q) quartet, (b) broad, (m) multiplet. The ligand H_4L[19] and the host−guest complex $(NEt_4)_7[NEt_4 \subset Ti_4L_6]$[24] were prepared as described in the literature. Solvents were degassed by sparging with N_2 for fifteen minutes. Mass spectrometry data were acquired using a Waters QTOF API mass spectrometer equipped with a Z-spray source. Molecular graphics were constructed in ORTEP-3[46] and Chimera[39,47] and rendered in POV-Ray.

4.2. Synthesis of Host−guest Complexes. 4.2.1. $(NBnMe_3)_{11}$[$NBnMe_3 \subset Ga_4L_6$] (Structure 4). To a degassed solution of H_4L (75 mg, 0.17 mmol) in MeOH (15 mL) was added benzyltrimethylammonium hydroxide (0.34 mmol as a standardized solution ion H_2O), and this yellow solution was again degassed and stirred and under N_2. To this yellow solution was added $Ga(acac)_3$ (41 mg, 0.11 mmol). The solution turned deeper yellow upon addition. This solution was again degassed and stirred under nitrogen for 18 h. The volume of the solution was then concentrated to 2 mL, and acetone was added (20 mL) to precipitate a fluffy, yellow solid. This was separated by centrifugation from the yellow filtrate and residual solvents were removed in vacuo. ^{1}H NMR: δ 13.37 (s, 12H, N*H*), 8.06 (d, J = 7.6, 12H, Ar*H*), 7.60 (d, J = 8.4, 12H, Ar*H*), 7.46 (m, 12H + 44H, exterior Bn*H* and cluster Ar*H*), 6.99 (m, 12H + 11H, exterior Bn*H* and cat*H*), 6.20 (d, J = 6.0, 12H, cat*H*), 6.13 (d, J = 7.6, 12H, cat*H*), 5.39 (br t, 1H, Ar*H* interior), 4.96 (br d, 2H, Ar*H* interior), 4.10 (br d, 22H, exterior CH_2), 3.86 (d, J = 7.6, 2H, Ar*H* interior), 2.94 (s, 99H, exterior CH_3), 0.26 (br m, 2H, interior CH_2), −0.43 (s, 12H, interior CH_3). ESIMS(−) (MeOH), ♦ = $[Ga_4L_6]^{12-}$, ◊ = $BnNMe_3^+$ calcd (found), *m/z*: 1041.0 (1042.4) [♦ + ◊ + 5Na$^+$ + 2H$^+$]$^{3-}$, 775.0 (776.3) [♦ + ◊ + 6Na$^+$ + 2H$^+$]$^{4-}$, 615.0 (616.3) [♦ + ◊ + 4Na$^+$ + 2H$^+$]$^{5-}$. X-ray quality single crystals of the dodeca(benzyltrimethylammonium) salt were obtained by slow diffusion of acetone into a wet DMF (with some DMSO to help dissolve the cluster) solution of the complex.

4.2.2. $(NH_2Me_2)_5(Cp_2Co)_2$[$Cp_2Co \subset Ti_4L_6$] (Structure 5). The H_4L ligand (14.5 mg, 0.035 mmol), Ti(O^{i}Pr)$_4$ (5.56 μL, 0.021 mmol), and $[CoCp_2][PF_6]$ (4.99 mg, 0.015 mmol) were combined in 600 μL of DMF-d_7. The solution was degassed and sealed under an atmosphere of nitrogen in a J-Young NMR tube. The reaction was heated at 145−150 °C in an oil bath. At the selected time points, the sample was removed and cooled to room temperature for ^{1}H NMR analysis (See Supporting Information). ^{1}H NMR (400 MHz, DMF-d_7): δ 8.37 (d, J = 7.0 Hz, 12H, *aryl*), 7.93 (d, J = 8.0 Hz, 12H, *aryl*), 7.67 (d, J = 8.3 Hz, 12H, *aryl*), 7.35 (t, J = 7.7 Hz, 12H, *aryl*), 7.15 (d, J = 6.9 Hz, 12H, *aryl*), 6.47 (t, J = 6.9 Hz, 12H, *aryl*), 5.73 (s, 20H, Cp-H exterior), 2.21 (s, 10H, Cp-H enaps.).

4.2.3. $K_9(Cp^*_2Co)_2$[$Cp^*_2Co \subset Ga_4L_6$] (Structure 6). The H_4L ligand (91.5 mg, 0.212 mmol), $Ga(acac)_3$ (52.0 mg, 0.140 mmol), and $[CoCp^*_2][PF_6]$ (66.0 mg, 0.140 mmol) were suspended in methanol (50 mL), and the solution was degassed by bubbling nitrogen though it for 15 min. A 1.0 M methanolic solution of KOH (450 μL, 0.450 mmol) was then added, and the solution was degassed for another 15 min. The reaction mixture was stirred overnight at room temperature, at which point some precipitate had formed. The solvent was removed under reduced pressure; the yellow residue was stirred vigorously with 15 mL of acetone and filtered, and the residual solvents were removed under vacuum to yield a yellow powder. ^{1}H NMR (500 MHz, 5:1 DMSO-d_6/MeOH-d_4): δ 13.32 (s, 4H, NH), 12.85 (s, 4H, NH), 12.83 (s, 4H, NH), 8.28 (overlapping m, 8H, *aryl*), 7.81 (d, J = 7.5 Hz, 4H, *aryl*), 7.40 (d, J = 7.5 Hz, 4H, *aryl*), 7.30 (d, J = 7.5 Hz, 4H, *aryl*), 7.19 (d, J = 7.5 Hz, 4H, *aryl*), 7.12 (overlapping d, J = 8.0 Hz, 8H, *aryl*), 6.76 (d, J = 7.5 Hz, 4H, *aryl*), 6.66 (overlapping m, 8H, *aryl*), 6.29 (d, J = 7.0 Hz, 4H, *aryl*), 6.21 (overlapping m, 4H, *aryl*), 6.18 (t, J = 7.0 Hz, 4H, *aryl*), 1.58 (s, 90H, 3Cp$^*_2$Co$^+$), −0.72 (s, 30H, Cp$^*_2$Co$^+$ encaps.). TOF MS ES(−) (MeOH/DMSO), ♦ = $[Ga_4L_6]^{12-}$, ◊ = Cp$^*_2$Co$^+$ calcd (found), *m/z* 1449.898 (1449.902) [♦ + 4◊ + 5K$^+$]$^{3-}$, 1353.152 (1353.168) [♦ + 3◊ + 6K$^+$]$^{3-}$, 1256.429 (1256.433) [♦ + 2◊ + 7K$^+$]$^{3-}$, 1149.703 (1159.700) [♦ + ◊ + 8K$^+$]$^{3-}$, 1077.677 (1077.683) [♦ + 4◊ + 4K$^+$]$^{4-}$, 1005.140 (1005.135) [♦ + 3◊ + 5K$^+$]$^{4-}$, 932.576 (932.584) [♦ + 2◊ + 6K$^+$]$^{4-}$, 850.531 (850.541) [♦ + ◊ + 7K$^+$]$^{4-}$, 796.308 (796.315) [♦ + 3◊ + 4K$^+$]$^{5-}$, 738.269 (738.277) [◊ + 2◊ + 5K$^+$]$^{5-}$, 680.215 (680.236) [♦ + ◊ + 6K$^+$]$^{5-}$.

4.3. Crystallographic Data. The diffraction data for structures **4** and **5** were collected on a Siemens SMART CCD[48] area detector with graphite-monochromated Mo Kα radiation. The data for the structures **3** and **6** were collected at the Advanced Light Source (ALS beamline 11.3.1) (Lawrence Berkeley National Laboratory, Berkeley, CA) using monochromated synchrotron radiation (λ = 0.77490 Å). Data were integrated by the program SAINT[49] and corrected for Lorentz and polarization effects. Data were analyzed for agreement and possible absorption using XPREP.[50] An empirical absorption correction based on the comparison of redundant and equivalent reflections was applied using SADABS.[51] Equivalent reflections were merged, and no decay correction was applied. Structures **3**, **5**, and **6** were solved by direct methods (SIR92),[52] and structure **4** was solved using Patterson methods (PATSEE)[53]

(46) Farrugia, J. L. *J. Appl. Crystallogr.* **1997**, *30*, 565.
(47) Pettersen, E. F.; Goddard, T. D.; Huang, C. C.; Couch, G. S.; Greenblatt, D. M.; Meng, E. C.; Ferrin, T. E. *J. Comput. Chem.* **2004**, *25*, 1605–1612.
(48) *SMART: Area-Detector Software Package*, version 5.059; Bruker Analytical X-ray Systems, Inc.: Madison, WI, 1995−1999.
(49) *SAINT: SAX Area-Detector Integration Program*, version 7.07B; Siemens Industrial Automation, Inc.: Madison, WI, 2005.
(50) *XPREP: Part of the SHELXTL Crystal Structure Determination Package*, version 6.12; Bruker AXS Inc.: Madison, WI, 1995.
(51) Sheldrick, G. *SADABS: Siemens Area Detector Absorption Correction Program*, version 2.10; University of Göttingen: Göttingen, Germany, 2005.
(52) For SIR92, see: Altomare, A.; Cascarano, G.; Giacovazzo, C.; Guagliardi, A. *J. Appl. Crystallogr.* **1993**, *26*, 343–350.
(53) Egert, E.; Sheldrick, G. *Acta Crystallogr.* **1985**, *A41*, 262–268.

in WinGX.[54] The structures were refined using Fourier techniques using SHELXL-97.[55] Hydrogen atoms were included but not refined. Hydrogen atoms on disordered Cp_2Co^+, $Cp^*_2Co^+$, NEt_4^+ or solvent were not included. Hydrogen atoms were positioned geometrically, with C−H = 0.93 Å for C_{arom}−H groups, C−H = 0.97 Å for CH_2 groups, and N−H = 0.89 Å and constrained to ride on their parent atoms. U_{iso}(H) values were set at 1.2 × U_{eq}(C) for all H atoms. For structures **3** and **6**, the electron density of the pockets of disordered solvent were calculated in Platon by the method of Spek.[56] In all cases, the electron density was sufficient to account for any counterions that were not explicitly located. A discussion of the data refinement and disorder modeling for each structure is included in the Supporting Information.

(54) For Wingx, version 1.70.01, see: Farrugia, L. J. *J. Appl. Crystallogr.* **1999**, *32*, 837–838.
(55) Sheldrick, G. M. *SHELX97: Programs for Crystal Structure Analysis*, release 97−2; Institut für Anorganische Chemie der Universität: Göttingen, Germany, 1998.
(56) Spek, A. L. *J. Appl. Crystallogr.* **2003**, *36*, 7–13.

Acknowledgment. We thank Dr. Frederick Hollander at the CHEXRAY facility for helpful discussions regarding crystallography, Dr. Ulla N. Andersen and Ákos Kókai for obtaining ESI-MS data, and Dr. Kathleen Durkin at the UCB Molecular Graphics Facility (NSF grant CHE-0233882) for assistance with volume calculations. This research and the ALS are supported by the Director, Office of Science, Office of Basic Energy Sciences (OBES), and the OBES Division of Chemical Sciences, Geosciences, and Biosciences of the U.S. Department of Energy at LBNL under Contract No. DE-AC02-05CH11231 and an NSF predoctoral fellowship to M.D.P.

Supporting Information Available: Crystallographic data, including crystallographic information files (CIF), a discussion of the disorder modeling, ^{1}H NMR spectra of **5**, and avi files showing the void spaces of compounds **1**−**6**. This material is available free of charge via the Internet at http://pubs.acs.org.

IC8012848